Electrical properties of partially saturated sandstones: Novel computational approach with hydrogeophysical applications

A. Brovelli,[1] G. Cassiani,[2] E. Dalla,[1] F. Bergamini,[1] D. Pitea,[1] and A. M. Binley[3]

Received 1 September 2004; revised 3 May 2005; accepted 11 May 2005; published 17 August 2005.

[1] Electric and electromagnetic geophysical tools are suitable methods for investigating moisture content, transport, and storage properties of the subsoil with noninvasive surveys. Interpretation of field data is still based on empirical or semiempirical equations, which must be calibrated with complex, time-consuming laboratory measurements. In this paper we develop pore-scale models suitable for computing the effective electric conductivity and the effective permittivity of partially saturated porous media on the basis of simple structural parameters (grain size distribution and porosity). We compute the electrical conductivity with three approaches that model the conductivity of the shell of coating clay around solid grains of shaly sandstones using different assumptions. We compare the simulated results with experimental data from Sherwood Sandstone (UK) and discuss the effect of these assumptions on the effective conductivity. Simulations performed using a modeling approach that accounts for interaction between volume and surface conduction show an excellent agreement with experimental data. We also model the effective permittivity of the same porous medium at several saturation values and obtain a good match with laboratory measurements.

Citation: Brovelli, A., G. Cassiani, E. Dalla, F. Bergamini, D. Pitea, and A. M. Binley (2005), Electrical properties of partially saturated sandstones: Novel computational approach with hydrogeophysical applications, *Water Resour. Res.*, *41*, W08411, doi:10.1029/2004WR003628.

1. Introduction

[2] The study of the subsoil through non invasive techniques has recently assumed a great importance for a wide range of disciplines, such as hydrogeology, waste disposal monitoring and hydrocarbon research [*Daily et al.*, 1992; *Kalinski et al.*, 1993; *Benson et al.*, 1997; *Chan and Knight*, 1999]; at the same time it remains a very complex problem due to both the difficulty in interpreting experimental data and in understanding phenomena that occur in the subsurface. In particular, in order to investigate the soil and the vadose zone, electromagnetic tools, such as time domain reflectometry (TDR) and ground-penetrating radar (GPR) have been employed, sometimes coupled with electrical resistivity surveys, because of the sensitivity of resistivity and dielectric permittivity to volumetric moisture content. Measurements performed using such techniques can be carried out both from surface and from borehole and are particularly suitable to characterize field heterogeneities. These data can also be used as input in numerical models developed to evaluate flow and solute transport in the vadose zone [*Binley et al.*, 2002a, 2002b; *Kowalsky et al.*, 2004; *Cassiani et al.*, 2004].

[3] Interpretation of data obtained from surveys with electric and electromagnetic tools is still generally based on empirical or semiempirical relationships, such as Archie's equation [*Archie*, 1942] or the *Waxman and Smits* [1968] model, which relate effective electrical conductivity to porous medium properties, or such as the complex refractive index method (CRIM) used for dielectric properties [*Roth et al.*, 1990]. Experimental measurements have shown that the effect of negatively charged grain-water interfaces on effective electrical conductivity and permittivity of porous media can be significant [*Waxman and Smits*, 1968; *Knight and Nur*, 1987; *Taylor and Barker*, 2002; *West et al.*, 2003]. The main phenomena involved are the grain surface polarization and the additional electrical conductivity caused by the electrical double layer. Both are not well understood and therefore difficult to model.

[4] A relatively large number of experimental and theoretical studies about the electrical response of fully saturated porous media exist [*Sen et al.*, 1981; *Bussian*, 1983; *Clavier et al.*, 1985; *De Lima and Sharma*, 1990; *Revil and Glover*, 1997; *Glover et al.*, 2000; *Chinh*, 2000; *Jones and Friedman*, 2000]. The effective conductivity of a fully saturated porous medium is generally related to the fluid conductivity (σ_w), pore geometry, connectivity and surface conductivity [*Clavier et al.*, 1985; *Korringa*, 1984; *Guéguen and Palciauskas*, 1994]. Most of the proposed models represent porous media as a system of two resistors in parallel and compute the effective conductivity as a sum of the effective conductivity of the water in the pore space

[1]Department of Environmental Science, University of Milano-Bicocca, Milan, Italy.
[2]Department of Geology and Geosciences, University of Milano-Bicocca, Milan, Italy.
[3]Department of Environmental Science, University of Lancaster, Lancaster, UK.

0043-1397/05/2004WR003628

and the surface conductivity. The latter is related to the properties of the grain coating, mainly composed of clay and oxides, and of the electrical double layer in contact with an aqueous solution.

[5] With regard to effective permittivity, many studies have been carried out to investigate the relationship between the effective permittivity of the medium and the water content. One approach is to use effective medium theories, as reviewed by [*Chelidze and Guéguen*, 1999]. Several new models have been proposed using such approximation in the very last years [e.g., *Robinson and Friedman*, 2003]. *Friedman* [1998] proposes a saturation-dependent model for the effective dielectric constant where the role of the water films is studied. A different approach is CRIM, which is a volume averaging relationship and explicitly incorporates porosity, volumetric water content and the dielectric constant of solid matrix, air and water phase [*Roth et al.*, 1990; *Chan and Knight*, 1999]. *Topp et al.* [1980], using a large set of different soils, developed an empirical relationship, which relates the effective permittivity to the volumetric water content and takes no account of variations in the properties of the solid matrix (e.g., permittivity, porosity, connectivity, etc.).

[6] The main goal of this paper is to demonstrate that the electrical response of a partially saturated porous medium, both in terms of DC conductivity and permittivity, can be simulated by adopting a unified conceptual approach, based on elementary principles and easy-to-measure medium properties (grain size distribution and porosity). Pore-scale models are powerful tools to investigate constitutive relations in porous media, because they provide fundamental understanding of pore-scale processes, which in turn can be incorporated into constitutive theories for the large-scale behavior. To our knowledge, few pore-scale studies of the electrical properties of unsaturated soils have been reported [*Endres and Knight*, 1991; *Suman and Knight*, 1997; *Tsakiroglou and Fleury*, 1999; *Kuntz et al.*, 2000; *Man and Jing*, 2001], and in most cases reconstruction of the porous medium is approximated (e.g., using network models).

[7] We present and compare three different approaches all based upon a digital representation of an experimental system. All these approaches solve the steady state electrical continuity equation in the digital domain in order to compute the electrical effective conductivity.

[8] 1. In the first approach, the electrical direct current flows through the volume of the porous medium, in the water phase and in the solid matrix. We introduce a fictitious matrix conductivity to account for surface conductivity.

[9] 2. In the second approach, we compute the electrical current flowing through two different disconnected domains acting in parallel: the volume of the water phase and the surface of the digital porous medium grains.

[10] 3. In the third approach we model the electrical interaction between water phase and solid matrix surface, and we compute the electrical direct current in a unified digital domain.

[11] Finally, we apply the code developed for approach 1 to compute the effective permittivity of the medium. Simulation results for all approaches are compared with experimental data from a U.K. semiconsolidated sandstone.

[12] It must be pointed out that the method presented in this paper is not intended as a substitute for empirical and/or physical-based relationship that can readily link electrical properties of a porous medium, e.g., to water saturation. On the contrary, our work is aimed at investigating the value and robustness of such relationships, particularly by analyzing the impact of assumptions of small (pore) scale mechanisms and properties on the macroscale response of the medium.

2. Background

[13] Few theoretical studies investigate the effects of water saturation, and most of the existing models take into account the decreasing water content using the same approach as in the original equation by *Waxman and Smits* [1968]. Similar to Archie's law, the Waxman and Smits model introduces a saturation exponent, n, and defines a power law relationship between the effective conductivity at full water saturation, $\sigma_e(s_w = 1)$, and effective conductivity, σ_e, at saturation s_w:

$$\sigma_e(s_w) = s_w^n \cdot \sigma_e(s_w = 1) \tag{1}$$

On the basis of experimental results, this model assumes that the concentration of counterions (and thus the conductivity of the electrical double layer), increases with decreasing water saturation:

$$\sigma_e(s_w) = \frac{s_w^n}{F}\left(\sigma_w + \frac{\sigma_s}{s_w}\right) \tag{2}$$

where F is the non dimensional formation factor (a function of porosity and pore connectivity), σ_s is the surface conductivity, expressed in S/m, that depends also on the electrical properties of the clay shell coating the sandstone grains (Figure 1). The specific conductance, Σ_s, [S], can be defined as

$$\Sigma_s = \int_{\chi_c} (\sigma(\chi) - \sigma_w) d\chi \tag{3}$$

where $\sigma(\chi)$ is the local conductivity, χ is the local coordinate normal to the grain surface, χ_c is the summed thickness of the shell of clay around the grain and of the electrical double layer, and σ_w is the water conductivity [S/m], assumed constant in the pore space. Note that it is very hard to measure or estimate the length χ_c, but it is possible to assume that the thickness of the clay coating is negligible with respect to the grain radius. A reasonable estimate for the thickness of the EDL, with natural, nonsaline groundwater, is 30–80 *Å* [*Guéguen and Palciauskas*, 1994]: this value is also negligible compared with the thickness of the clay shell. *O'Konski* [1960] demonstrates that for a sphere of radius R and specific surface conductivity Σ_s, immersed in a homogeneous medium, it is possible to compute the equivalent value of volume electrical conductivity, σ_s, as

$$\sigma_s = \frac{2\Sigma_s}{R} \tag{4}$$

Equation (4) has been extended to complex systems [*Johnson et al.*, 1986; *Revil et al.*, 1998], such as porous

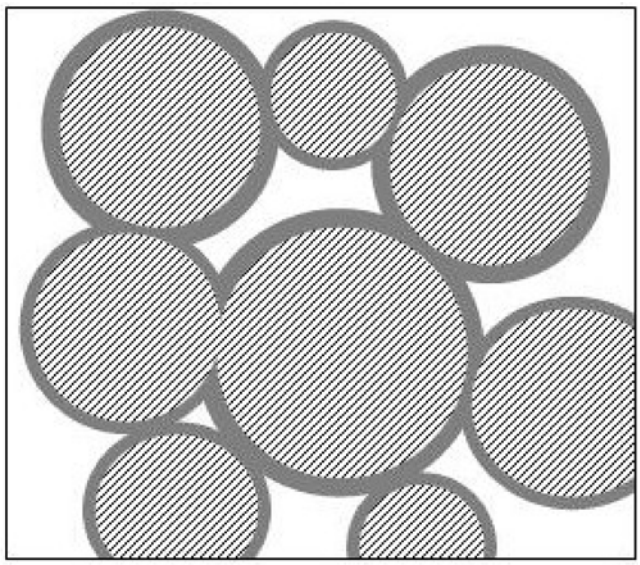

Figure 1. Idealized cross section of a shaly sandstone. The silica grains are coated by a film of clay and oxides (shaded in gray). The electrical double layer thickness around the clay is not shown.

media composed by a pore space and an insulating matrix coated with a film of colloids that produce a specific surface conductivity Σ_s. The choice of the scale length R is critical because it must describe correctly the microgeometry of the pores. *Revil et al.* [1998] used $R = \langle R_g \rangle$, where $\langle R_g \rangle$ is the mean grain radius. A more complex parameter proposed to characterize transport in porous media is the weighted pore volume to surface area [*Johnson et al.*, 1986], Λ, a measure of the interconnected porosity, defined by

$$\frac{\Lambda}{2} = \frac{\int |E(r)|^2 dV_p}{\int |E(r)|^2 dA_s} \tag{5}$$

where $E(r)$ is the electric field at point r in absence of surface conductivity, V_p is the volume of the pore space and A_s is the interfacial area. *Johnson et al.* [1986] derived an analogous relationship of equation (4) involving $R = \Lambda$, $\sigma_s = \frac{2\Sigma_s}{\lambda}$ and [*Wildenschild et al.*, 2000] verified its validity for unconsolidated sandstones with clay content varying from 0 to 10%. *Bernabé and Revil* [1995] pointed out that Λ is difficult to determine; however, in porous media with a negligible value of noninterconnected porosity, that does not contribute to transport, it is possible to assume [*Wildenschild et al.*, 2000; *Nettelblad et al.*, 1995]

$$\Lambda \approx 2\frac{V_p}{A_s} \tag{6}$$

[14] *Knight* [1991] studied the electrical response of partially saturated sandstones and showed that, with the same degree of water saturation, using low-frequency current different water phase geometries produce different effective DC conductivity, i.e., there is hysteresis of effective conductivity during imbibition and drainage. *Knight* [1991] points out that repeated cycles of wetting and drying can lead to complicated pore-scale distribution of the aqueous phase. Further, the effects of wetting phase films around the solid matrix seem to be very important on the DC/low frequencies effective response [*Knight*, 1991; *Endres and Knight*, 1991; *Berg*, 1995; *Chinh*, 2000]. All these effects of water saturation are not explicitly taken into account by the Waxman and Smits' model, so this model could fail in predicting effective conductivity in a porous medium where there is a complicate geometry of the water phase. In the model described in the following sections, the water phase distribution plays an important role in determining the effective conductivity and so it is possible to account for complicated geometries of this phase by creating a representative digital domain. However, we considered only the case of water saturation changes by drainage.

3. Methods

[15] The adopted pore-scale methodology is based on three sequential steps.

[16] 1. The first step is creation of a close packing of spheres with a prescribed grain size distribution and porosity, using the computer code developed by [*Yang et al.*, 1996]. The sphere packing is then digitized into a three dimensional cubic grid.

[17] 2. The second step is simulation of primary drainage in order to obtain phase distributions at several degrees of water saturation, using the morphological simulator by [*Hilpert and Miller*, 2001]. Each voxel (discrete element of volume) contains only one phase (solid matrix, water or air).

[18] 3. The third step is computation of electrical effective properties of the porous medium by solving the governing partial differential equations of the electrical field to compute (1) the electrical effective conductivity and (2) the effective permittivity.

[19] The ohmic current due to free charges (i.e., electrons or ions), $\vec{J}$, is defined as,

$$\vec{J} = \sigma\vec{E} = -\sigma\nabla V \tag{7}$$

while the electric displacement vector $\vec{D}$, as

$$\vec{D} = \epsilon\epsilon_0\vec{E} = -\epsilon\epsilon_0\nabla V \tag{8}$$

where $\vec{E}$ is the electric field, V is the electric potential, σ is the electrical conductivity, ϵ is the relative permittivity of the medium, ϵ_0 is the permittivity of the vacuum, 8.854×10^{-12} F/m [e.g., *Grant and Phillips*, 1990]. Applying the continuity equation to $\vec{J}$, at steady state, we obtain

$$\nabla \cdot \vec{J} = \nabla \cdot (\sigma\nabla V) = 0 \tag{9}$$

which is the ohmic current equation. A similar equation holds also for electrical current along the solid-fluid interface, in absence of electrical interaction between this surface and the phase volume, i.e., considering this interface as acting in parallel to the current flowing in the bulk volume:

$$\nabla \cdot (\Sigma_s \nabla V) = 0 \tag{10}$$

where ∇ is intended as a 2-D operator along the surface. The electrical displacement vector can be computed using [*Hilfer et al.*, 2000]:

$$\nabla \cdot \vec{D} = \nabla \cdot (\epsilon\epsilon_0 \nabla V) = \rho_f = 0 \tag{11}$$

with mean free charge density ρ_f in the voxel equal to zero.

[20] Equations (9), (10) and (11) are of the same form [*Guéguen and Palciauskas*, 1994] and a general expression can be considered:

$$\nabla \cdot (\alpha \nabla V) = 0 \tag{12}$$

where α can be set equal to σ, to Σ_s or to $\epsilon\epsilon_0$. Clearly, using this approach we cannot model the different tortuosities of cations and anions in the partially saturated porous medium, caused by the different pathway of the charge carriers. This approximation could have some implications in modeling the electrical conductivity, while is less crucial for the dielectric constant. We developed three different approaches to solving this general equation within the porous medium and along the surface between solid matrix and aqueous phase. We compared the simulated results against experimental data by *Binley et al.* [2002b] and *West et al.* [2003] in order to investigate the role of several parameters, particularly water saturation and clay conductivity. All simulations have been performed on an IBM R6000 Power4 machine, solving the system of linear algebraic equation using the routine DSRIS of the ESSL library (Engineering Scientific Subroutine Library) (IBM, ESSL for AIX V4.1, ESSL for Linux on pSeries V4.1 Guide and Reference). Note that equation (12) is totally equivalent to the PDE governing fluid flow in porous media. This fact leads to important parallelisms in terms of conceptualization and numerical approaches. For example, upscaling in porous media have long been investigated for fluid flow [e.g., *Durlofsky et al.*, 1997; *Chen et al.*, 2003], with obvious similarities to our approach.

3.1. Approach One: Fictitious Solid Conductivity

[21] *Dalla et al.* [2004] presented a finite difference, cell-centered, central difference, second-order approximation that solves the general, three-dimensional current equation in the volume of the porous medium (12). In this approach two opposites sides of the cubic digital domain have Dirichlet boundary conditions, with a prescribed potential; the other sides have no flow boundary conditions. At the voxel boundaries the electrical conductivity or permittivity between two adjacent voxels is computed as the harmonic mean between the conductivity of the voxels. The electrical potential is computed at the nodes of the mesh (the center of the voxels) by solving the system of linear algebraic equations, obtained by discretizating equation (12), with an iterative solver, preconditioning the system by a diagonal matrix, suitable for symmetric matrices. From the electrical simulated potential we compute the current intensity through the digital porous medium. Finally the effective electric conductivity is derived applying Ohm's law to the whole digital block. The main limitation of this approach is that the fictitious conductivity probably depends on the grain size (equation (4)), while in our model we adopt a constant value for all grains, which could be considered as the mean fictitious clay conductivity.

3.2. Approach Two: Resistors in Parallel

[22] In order to compute the effective electrical conductivity of a porous medium, it is usually assumed that the flow of charges takes place through two different resistors connected in parallel: one is the aqueous solution which fills the pore space, the other is the matrix-water interface. Following such an approximation, we compute the effective conductivity as

$$\sigma_e = \frac{(I_v + I_s)}{\Delta V} \frac{l}{S} \tag{13}$$

where σ_e is the effective conductivity, l, S are respectively the length and the cross section of the digital cubic sample, ΔV is the applied potential difference, I_v and I_s are respectively the current intensity in the water volume and on the interface.

[23] To obtain a tool more flexible than the one presented in section 3.1 for the computation of the electrical conductivity in the porous media, we developed a new finite element code that solves equation (12) in a three dimensional mesh composed by both 2-D quadrilateral and triangular elements connected in the 3-D space and 3-D linear cubic quadrilateral elements. We adopted the Galerkin finite element formulation. Dirichlet boundary conditions are applied to the nodes lying on two opposite faces of the cubic porous medium, and no flow boundary conditions are applied to the remaining four faces. The resulting system of algebraic equations is solved using the conjugate gradient method, which is suitable for positive definite symmetric matrices. We adopted preferentially a finite element approach primarily because of its flexibility in accommodating elements representing both the conductance through the bulk volume (3-D elements) and along the solid-pore interface (2-D elements), possibly connected to each other (as in our approach 3). In addition, a finite element mesh can be more easily designed to represent only the conducting phases, i.e., leaving out solid and gas insulator volumes, thus reducing the computational burden (see below). However, our numerical experiments show also that finite element, in our Bubnov-Galerkin formulation, are superior to our finite difference approach in terms of accuracy at solving the DC electrical current problem in a multiphase porous medium. In particular finite elements reach convergence to the discretization-independent limit computed using the Richardson's extrapolation (see *Dalla et al.* [2002] for an explanation on how this limit is computed) for relatively coarse discretization, while finite differences require a much finer discretization to achieve the same performance.

[24] Starting from the digital porous medium, two different digital domains are created, which represent (1) the volume of the porous medium and (2) the water-solid matrix interface. Since the solid (silica) matrix and the gaseous phase are electrical insulators, electrical current can only flow through the aqueous phase, which occupies a minor part of the total volume, even at full saturation. Consequently, in order to reduce the computational resources required by the code, we created a 3-D finite element mesh neglecting the insulator phases altogether. This operation

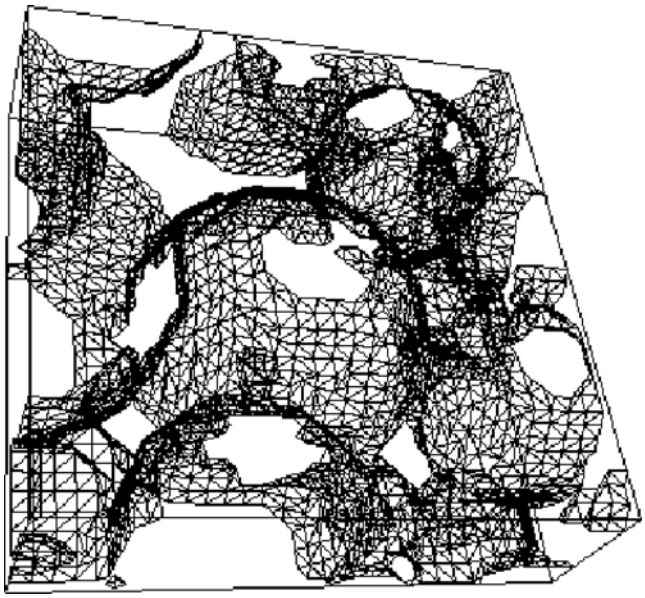

Figure 2. Example of a 3-D triangular mesh representing the solid matrix-water interface created using the standard marching cube algorithm. We show a 30 × 30 × 10 voxel subdomain, extracted from the digital porous medium used in numerical simulations.

produce a large reduction in the number of degrees of freedom of the system (about 48%); furthermore, the system matrix is better conditioned. The resulting mesh represents the volume of the water phase and permits the computation of the electrical current, I_v.

[25] In order to model the additional component of the electrical flux, I_s, due to (1) the coating clay layer and (2) the electrical double layer around it, we approximate the surface between solid matrix and aqueous phase, as the triangular mesh generated by the standard marching cube algorithm, developed by *Lorensen and Cline* [1987], that creates smoothed surfaces from three-dimensional digital images (e.g., for biomedical applications). *Dalla et al.* [2002] applied this algorithm to digital porous media in order to compute the interface area between the phases. They demonstrated that the values of interfacial area simulated with such an approach are comparable with experimental results, i.e., the surface generated by the code is representative of the real internal surface of a porous medium. The interface between solid matrix and aqueous phase modeled as a triangular irregular 3-D network (see Figure 2) is suitable for numerical simulation via our finite element code.

3.3. Approach Three: Joint Volume and Surface

[26] The model presented in section 3.2 is based on the assumption that volume and surface act in parallel. This is a strong approximation, because, in fact, surface and water volume are electrically connected and therefore they interact. In order to evaluate the importance of this approximation, starting from the digital porous medium, we created a different digital domain where the 3-D linear brick elements, and the 2-D elements are jointly considered in the same 3-D finite element mesh. In this new domain the volume is discretized exactly as in section 3.2, while the surface is composed by squared elements which form the matrix surface in the porous medium digitized with cubic elements, instead of the triangular mesh generated with the standard marching cube algorithm.

4. Simulated Phase Distributions

[27] We created a random packing of spheres with the computer code by *Yang et al.* [1996], honoring porosity and grain size distribution measured on several samples of Triassic Sherwood Sandstone extracted from an experimental site in South Yorkshire (UK). Table 1 reports the properties of the synthetic porous medium; the grain size distribution is assumed to be lognormal. Data on both electrical conductivity and permittivity as a function of water saturation are available for samples taken from the same site [*Binley et al.*, 2002b; *West et al.*, 2003].

[28] Primary drainage was simulated on a 384^3 voxels digital representation of the packing with a morphological simulator [*Hilpert and Miller*, 2001] which produce the phase distribution on the digital domain at different degrees of saturation. The simulated behavior was compared with laboratory measurements of primary drainage [*Dalla et al.*, 2004]. Figure 3 shows the simulated and experimental data. For $s_w > 0.20$ the agreement is very good; this indicates that the simulated phase distributions (solid, water, air) are representative of the real medium. For $s_w < 0.20$ there is a discrepancy between the experimental data set and the simulated curves, due to the residual water in the real porous medium, that cannot be modeled with the morphological simulator. This is a limitation of our model, that in future could be overcome by using, e.g., a Lattice-Boltzmann approach. The discretization and domain size effects on the digital sample were investigated, as reported by *Dalla et al.* [2004]. Following this analysis, the adopted digital packing can be considered as a representative elementary volume both for the drainage and for the electrical properties.

5. Electrical Conductivity Versus Water Saturation

[29] Experimental measurements of direct current (DC) effective electrical conductivity (σ_e) as a function of water saturation on Sherwood Sandstone are reported by *Binley et al.* [2002b]. The cores had been saturated with groundwater from Hatfield, and then desaturation had been performed with stepped evaporative drying. At each step the samples were equilibrated for 24 hours, weighted to recover the changes in moisture content and then the electrical conductivity was measured using a 4 electrodes setup. We fit their experimental data set using the resistivity index correlations proposed by [*Archie*, 1942] and [*Waxman and Smits*, 1968]

Table 1. Properties of the Simulated Sphere Packing

Parameter	Value	Unit
Grain radius R_g	0.073 ± 0.025	mm
Domain length L	3.987	mm
Porosity Φ	0.39	
Number of spheres	14501	
Specific surface area	16.95	1/mm

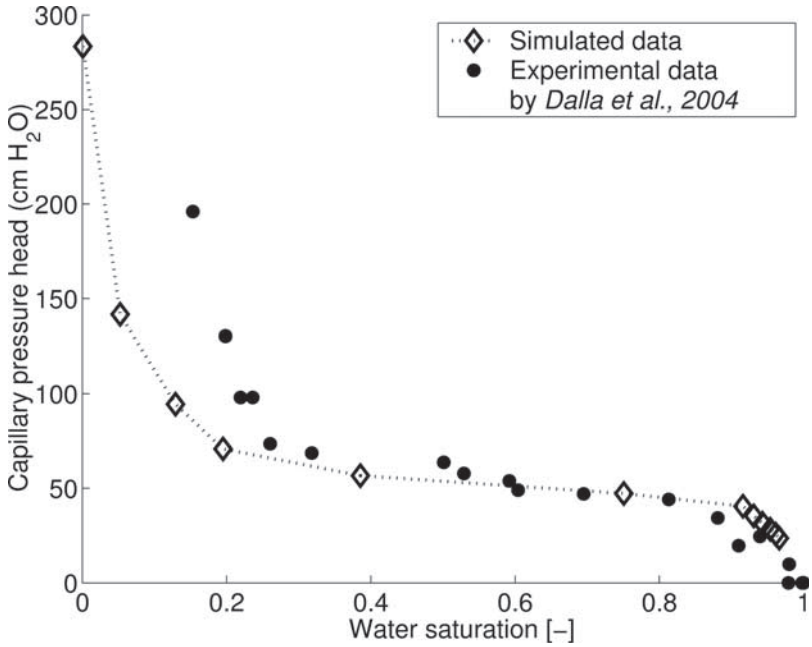

Figure 3. Comparison between experimental measurements and simulated data of the $p^c - s_w$ relationship by *Dalla et al.* [2004].

(reported as W-S). Results are shown in Figure 4. The main difference between the two models is that Archie's equation applies to porous media with negligible clay conductivity (e.g., with very low clay content) while the W-S model is commonly adopted to interpret DC electrical current behavior of shaly sand [*Waxman and Smits*, 1968]. The Archie's resistivity index (RI_A) and the W-S resistivity index (RI_{WS}) are defined as

$$RI_A = \frac{\sigma_e(s_w = 1)}{\sigma_e(s_w)} = s_w^{-n} \tag{14}$$

$$RI_{WS} = \frac{\sigma_e(s_w = 1)}{\sigma_e(s_w)} = s_w^{-n}\left(\frac{\sigma_w + BQ_v}{\sigma_w + BQ_v/s_w}\right) \tag{15}$$

where B is the equivalent conductivity of the compensating counterions ((Ω/m)/(meq/cm^3)) and Q_v is the concentration of counterions per unit pore volume (meq/cm^3).

[30] From the best fit of the experimental measurements with equation (14), we obtained $n = 1.18$. According to *Glover et al.* [2000], we assumed $\sigma_s = BQ_v$ in equation (15) and consequently the least squares best fit yielded $n = 1.58$ and $\sigma_s = 2.88 \times 10^{-2}$. Figure 4 shows the results of such best fit. Predictions with Archie's equation at low saturation deviates from experimental data, while the W-S model shows a marginally better agreement (determination coefficients are $r^2 = 0.967$ and $r^2 = 0.980$ respectively).

5.1. Approach One: Fictitious Solid Conductivity

[31] Our digital porous medium is composed of three potentially conducting phases: the aqueous phase (w), the solid matrix (m), and the gaseous phase (g). We assign $\sigma_w = 6.8 \times 10^{-2}$ S/m, which is the value of conductivity experimentally measured on the groundwater saturated Sherwood Sandstone samples. Air could be considered as an insulating phase, thus we adopt a value of conductivity such that flux of charges in such phase can be considered negligible, $\sigma_a = 1 \times 10^{-7}$ S/m, as discussed by *Dalla et al.* [2004]. Note that zero conductivity values cannot be used since they could produce a singular system matrix. The solid phase is also insulating, but we introduce a fictitious value of conductivity in order to account for clay conduction. Following Waxman and Smits, we assume surface conductivity increases with decreases of saturation:

$$\sigma_m(s_w) = \frac{\sigma_m(s_w = 1)}{s_w} \tag{16}$$

where $\sigma_m(s_w = 1)$, and $\sigma_m(s_w)$ are the matrix conductivity of the fully saturated porous medium and the matrix conductivity at water saturation s_w. We calibrate the value $\sigma_m(s_w = 1) = 1.43 \times 10^{-3}$ S/m, obtaining an effective conductivity of the digital porous medium equal to the measured conductivity on fully saturated samples. Further details of such approach are given by *Dalla et al.* [2004]. Results of simulations are reported in term of electrical effective resistivity, compared with experimental data in Figure 5. At $s_w \geq 0.4$, simulated data match the experimental data with excellent accuracy, while at lower water saturation the model underestimates the real resistivity values. This may be caused by a slight overestimation of solid matrix conductivity (see equation (16)) that is calibrated against real data at full saturation. As saturation decreases, the relative importance of current pathways through the solid increases, and the slight inaccuracy in solid matrix conductivity becomes apparent.

[32] At $s_w \geq 0.4$, simulated data well match the experimental measurements, while at lower water saturation the predicted resistivity is too lower than real data. This fact, according with equation (16), is probably due to the high value of matrix conductivity and thus a too high current

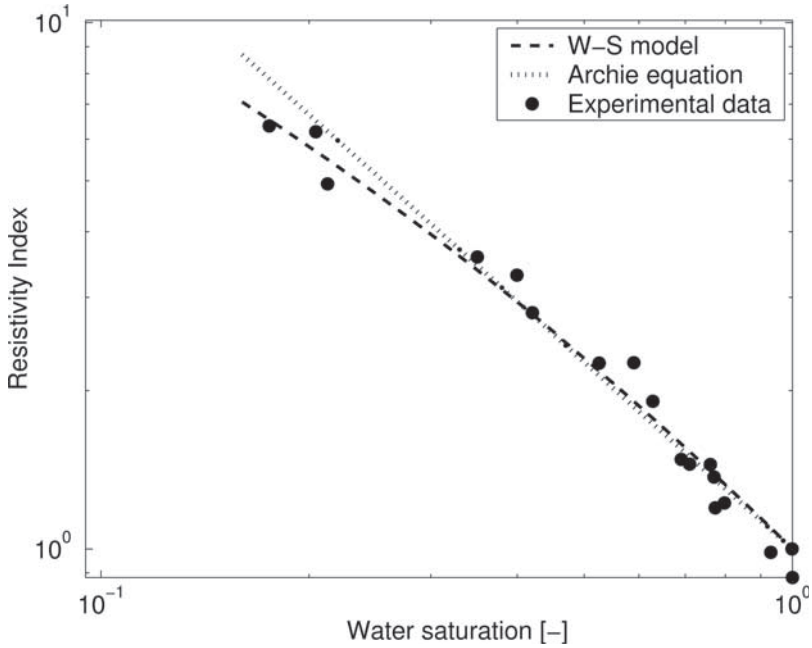

Figure 4. Log-log plot showing the resistivity index of the experimental measurements by *Binley et al.* [2002b] of effective electrical conductivity versus water saturation (circles), *Waxman and Smits*' [1968] equation (dashed line), and *Archie*'s equation [1942] (dotted line) best fit.

density through the solid matrix at low saturation. Note that the fictitious solid resistivity is obtained from matching experimental bulk resistivity at full saturation.

5.2. Approach Two: Resistors in Parallel

[33] In order to improve the approach presented in section 5.1, we solve the electrical current equations (equations (9) and (10)) in such domains, using the finite element computer code presented in section 3.2. This code is more expensive, in terms of memory requirement, than the one adopted in section 5.1, but has already pointed out in section 3.2: (1) a finite element formulation allows us to deal with more complicated domains, which can be composed by both 2-D and 3-D elements, as pointed out in section 3.2. Note, however, that the higher computational cost is partially balanced by neglecting the elements of non conductive phases, i.e., the solid matrix and the gaseous phase. (2) at the same domain discretization, the finite element formulation produce a lower numerical error with respect to that introduced by the finite difference scheme.

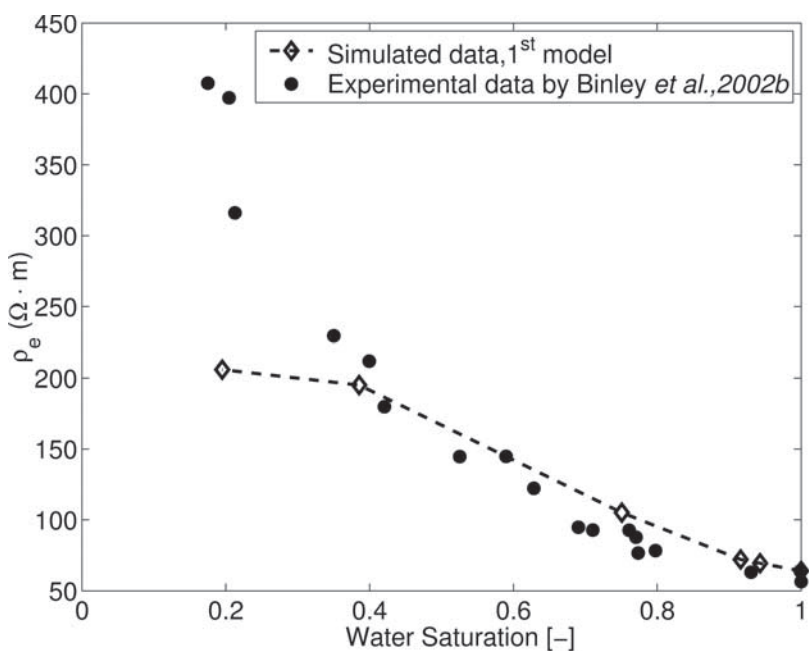

Figure 5. Plot of the effective resistivity ρ_e versus water saturation, approach 1: surface effects modeled using a fictitious matrix conductivity.

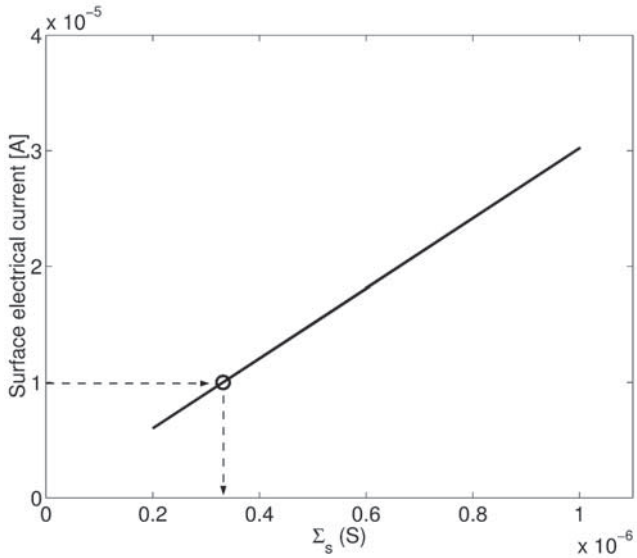

Figure 6. Electrical current along the surface (line) as a function of clay conductance (Σ_s). The circle indicates the calibrated value.

[34] The simulations were performed on an IBM R6000 Power4; the surface of a digital porous medium discretized with 384^3 voxels had about 14×10^6 nodes and required about 2 hours of CPU time. Because of the strong reduction in the number of degrees of freedom in the system's matrix, the second approach is computationally less expensive than the finite difference code: the computation (CPU) time required to simulate current flow through the water volume varies, depending on the saturation degree (13% to 100%), between 2h 30min and 3h 45min.

5.2.1. Clay Conductance Calibration

[35] In order to calibrate the value of clay conductance Σ_s, we compute the electrical current through the fully saturated digital porous medium, setting water conductivity $\sigma_w = 6.8 \times 10^{-2}$ S/m. The additional contribution of the surface conduction to the flow of charges has been computed by subtracting from the experimental value of electrical current the simulated electrical current in the water volume of the digital porous medium. Using the finite element code that simulates electrical current along the solid-fluid interfaces, we obtained the value of surface conductance Σ_s that yields the best match of experimental specimen resistivity at full saturation, and we obtained $\Sigma_s = 3.32 \times 10^{-7}$ S (Figure 6).

[36] The digital porous medium we analyze has $\langle R_g \rangle = 0.073$ mm (see Table 1) and the pore space is almost completely interconnected, so we can apply equation (6) and we obtain $\Lambda = 4.62 \times 10^{-5}$ m. From equation (4), using the value Σ_s calibrated and setting $R = \langle R_g \rangle$ and $R = \Lambda$, we compute $\sigma_s = 0.91 \times 10^{-2}$ S/m and $\sigma_s = 1.44 \times 10^{-2}$ S/m, respectively. The experimental value, obtained as the best fit of experimental data with [*Waxman and Smits*, 1968] equation, is $\sigma_s = 2.88 \times 10^{-2}$ S/m; thus the value obtained from pore-scale modeling is in the range predicted by empirical relationships, even though the difference amounts to a factor between 2 and 3. From experimental measurements on different samples of Ottawa sand with a dispersed clay content in the range 0%–10%, *Wildenschild et al.* [2000] obtained 2×10^{-7} S $\leq \Sigma_s \leq 8.5 \times 10^{-7}$ S; *Nettelblad et al.* [1995], for artificially made clay-free sandstones, found 0.5×10^{-7} S $\leq \Sigma_s \leq 1.5 \times 10^{-7}$ S. The value we obtain from our simulations, $\Sigma_s = 3.32 \times 10^{-7}$ S, is well within the above range, for a sandstone with a low clay content.

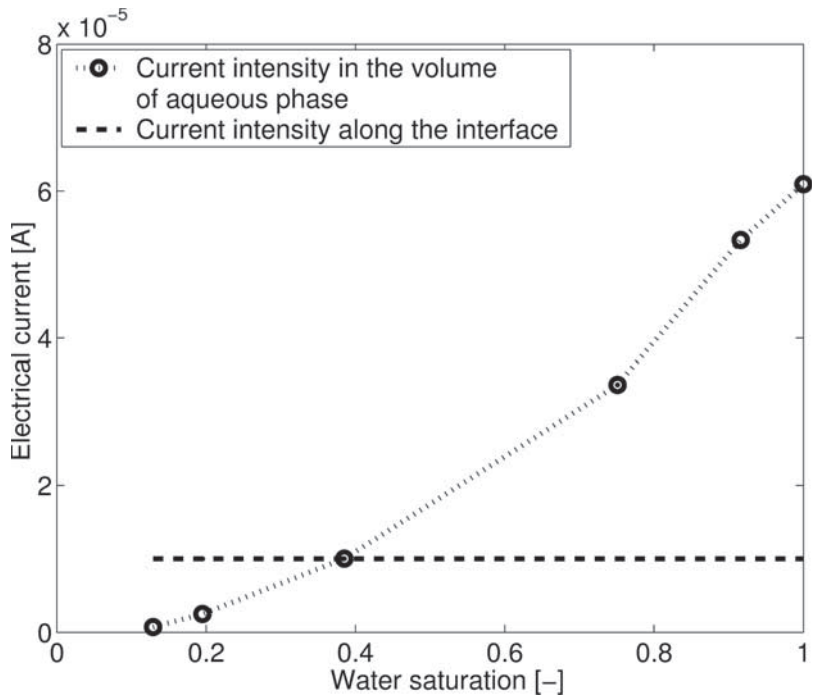

Figure 7. Relationship between electrical current intensity and water saturation. At $s_w \leq 0.4$ the equivalent conductivity is mainly due to interface.

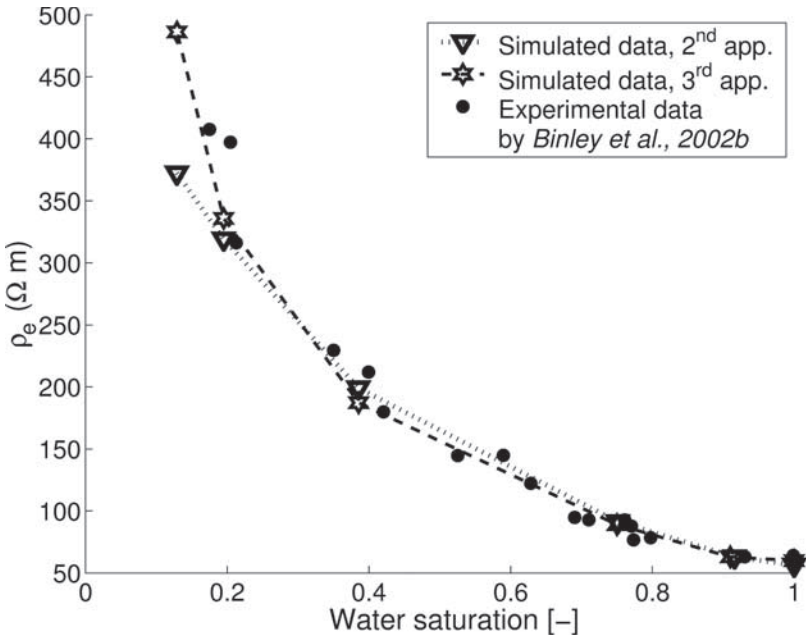

Figure 8. Comparison between simulated data of approach 2, approach 3, and experimental data.

5.2.2. Effective Conductivity: Simulation and Comparison With Experimental Data

[37] We assume Σ_s, and thus I_s, to be constant at each value of s_w; this is justified because, for $s_w > 0.15$, the thickness of the wetting phase films around matrix is larger than the Debye length, the thickness of the electrical double layer, so changes in water content do not modify the physical-chemical properties of the electrical double layer and also the films remain interconnected and ensure electrical conductivity. Figure 7 shows the contribution of the charge flow through both the surface and the volume to the total current, as a function of water saturation: from our simulations it is apparent that for $s_w > 0.5$ the current is mainly channelled through the pore water, while for $s_w < 0.5$, the contribution of the electrical double layer to the total flow becomes comparable and prevalent at smaller s_w.

[38] A comparison between simulated effective conductivities and experimental data from *Binley et al.* [2002b] is shown in Figure 8. These simulated results show an excellent agreement with experimental data set, particulary at $s_w \geq 0.2$. The simulated curve is very close to the experimental one; this may be taken as evidence that keeping clay conductance constant is correct, at least at $s_w \geq 0.15$, while as previously discussed, the commonly adopted Waxman and Smits equation assumes that clay conductivity is a function of water saturation in the whole range of s_w. The predicted resistivity of the porous medium with the lowest water saturation, $s_w = 0.13$, is lower than the value of the corresponding experimental data. A possible reason for this discrepancy is that we approximate the porous medium with two different, noninteracting domains.

5.3. Approach Three: Joint Volume and Surface

[39] In the previous section we investigated the assumption that the porous medium behaves as a system composed of two resistors in parallel. This approximation appears to be correct, at least at $s_w \geq 0.2$ for the data set used in this paper, having a low clay content. In the third approach we join the two different domains, the volume of the water phase and the solid-water interface, and thus we model their electrical interaction. We obtain a single digital domain composed by 2-D squared elements and 3-D linear bricks. Because we use the same finite element discretization of approach 2 and the digital domains are quite similar, the CPU time required is comparable with that reported in section 3.2.

[40] Using the same finite element code adopted in section 3.2, we calibrate a value of surface conductance on the fully saturated porous medium. We obtain $\Sigma_s = 1.3 \times 10^{-7}$ S, a value that is about 2.5 times smaller than the value calibrated and discussed in section 5.2. Reasons for such difference are as follows. (1) The total surface area computed with approach 3 is higher than the value computed using the standard marching cube adopted in approach 2. Note that this is a numerical issue that depends on the methods we adopt to discretize the grain surface. From the physical point of view, surface conductance is linearly proportional to the surface area in quartz-based media [*Revil and Glover*, 1997]. (2) The effects of the grain coating and of the electrical double layer, electrically connected with the water in the pore space, produce a decrease in the calibrated value. Nevertheless, the two calibrated values are of the same order of magnitude.

[41] Figure 8 reports also the results of the simulations with this approach, compared with experimental data by *Binley et al.* [2002b]. Simulated data show excellent agreement with the experimental ones at any value of water saturation, while at $s_w < 0.2$ approach 2 fails. This could indicate that the assumption of two resistances in parallel is not appropriate in porous media with a high clay conductance, because the interaction between the water phase and the grain-water surface could produce an increasing in

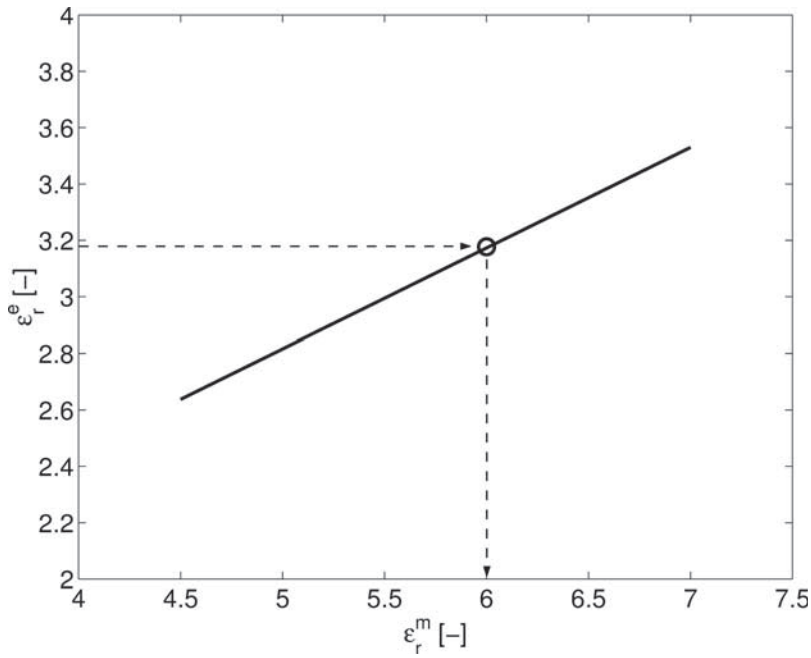

Figure 9. Calibration of matrix relative permittivity on the digital porous medium with $s_w = 0$.

electrical connectivity, and thus in electrical effective conductivity, as pointed out by *Chinh* [2000].

6. Permittivity Versus Water Saturation

[42] *West et al.* [2003] report on a data set of experimental measurements of electrical permittivity on several samples of Sherwood Sandstone and on a wide range of frequencies, collected at the same site of the samples presented in section 5. Using a coaxial cell, they measure both the real and imaginary parts of the effective permittivity and demonstrate that, in the frequency range 300–1000 MHz, the real effective dielectric constant ϵ_e^r is largely independent of frequency, while below 350 MHz ϵ_e^r of fine-grained, clay-rich sandstone shows frequency dispersion. We choose to compare our simulated data with the experimental results measured at frequency of 300 MHz and 500 MHz on the sample labeled as B5(H) by *West et al.* [2003], because it has structural parameters that match closely those of our simulated packing: nonlaminated, porosity 35.8%, d_{50} = 191 μm.

[43] To model real effective permittivity, we use the same finite difference code developed for approach 1 (section 3.1). We do not use the finite element code, as in approach 2 and 3, because permittivity depends on the three phases of the porous medium (water, solid matrix and air). This means that we cannot neglect, as for the electrical conductivity, the nodes of solid matrix and gaseous phase. This in turn produces a large increase in the required computational resources. On the basis of the results in section 6.2, the numerical error introduced by finite differences appears to be negligible.

6.1. Matrix Permittivity Calibration

[44] Using the finite difference code described for approach 1 above, we studied the $\epsilon_r^e - \epsilon_r^m$ relationship on the dry porous medium in order to evaluate the value of matrix permittivity to adopt when studying the behavior of effective permittivity varying water saturation. We adopt air relative permittivity $\epsilon_r^a = 1$, and we investigate the effects of matrix permittivity varying from $\epsilon_r^m = 4.5$ to $\epsilon_r^m = 7$, which is the range of solid phase permittivity usually found in natural porous media [*Guéguen and Palciauskas*, 1994]. The value of solid matrix relative permittivity which matches experimental data on the dry porous medium is $\epsilon_r^m = 6$ (see Figure 9), which is a typical value for silica sands with a significant content of clays (ϵ_r^m 5.5–5.8) and other impurities, such as oxides (e.g., hematite $\epsilon_r^m = 18.1$), carbonates ($\epsilon_r^m = 9.1$), etc. [*Robinson and Friedman*, 2003].

6.2. Simulations and Comparison With Experimental Data

[45] We perform simulations on the previously created digital porous medium at different water saturations and compare simulation results with experimental data of effective relative permittivity measured by *West et al.* [2003]. As permittivity of the three phases, we adopt $\epsilon_r^m = 6$, $\epsilon_r^a = 1$, as in section 6.1, and water relative dielectric constant ϵ_r^w = 80.1, as proposed by *West et al.* [2003].

[46] As shown in Figure 10, the simulated data match well the experimental data set, at any value of moisture content. This indicates that (1) the role of surface polarization is negligible or could be included in the matrix permittivity, (2) the wetting films, that are currently not modeled by our approach, do not contribute much to the effective electrical permittivity, while they play an important role in determining effective conductivity. Simulated results match the experimental data at 500 MHz slightly better than the data at 300 MHz. The reason for this is that the frequency of 300 MHz is close to the frequency range where data by *West et al.* [2003] are affected by

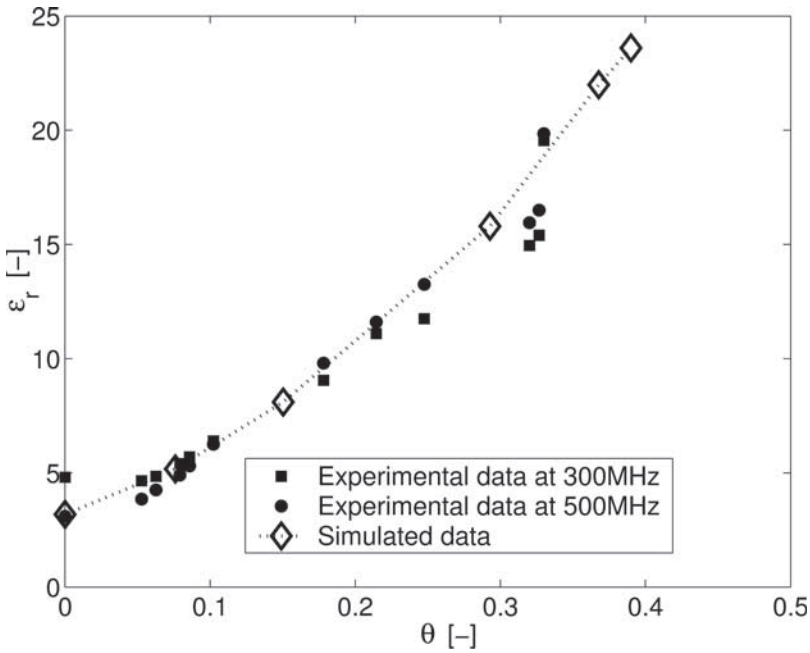

Figure 10. Experimental (dots and squares) [*West et al.*, 2003] and simulated (diamonds) data of relative effective permittivity ϵ_r^e versus the volumetric moisture content, θ.

dielectric dispersion, while at 500 MHz there is no dielectric loss.

[47] Most important, we are able to reproduce measured real permittivity values using the same conceptual framework used for simulating DC conductivity.

7. Summary and Conclusions

[48] In this work we presented pore-scale models able to evaluate both effective electrical conductivity and effective permittivity of a partially saturated porous medium in a unified conceptual framework. Simulation domains are created on the basis of simple structural parameters (grain size distribution and porosity) of an experimental porous medium. With regard to the effective electrical conductivity, we developed three different models, each based upon a different approach to model clay conductivity. In the first approach we modeled the clay conductivity as a fictitious matrix conductivity, which depends on the degree of water saturation, as proposed by Waxman and Smits. Applying this model, we obtained a good match with experimental data with water saturation in the range 0.4–1. Below s_w = 0.4, the predicted resistivity becomes too low. In the second approach we created a triangular mesh that represents the interface between the solid matrix and the water phase. Following the assumption that the porous medium behaves as a system of two resistors in parallel, we computed the effective conductivity from the sum of the current flowing along the grains surface and that flowing in the volume of the water phase. We assumed surface conductivity is constant. The simulated results show excellent agreement with the experimental data set, at least at $s_w \geq 02$. Finally, we introduced a third model where current is simulated in a single domain, created by joining the volume of the water phase and the surface of solid matrix in the porous medium. Using this third approach, the match between the simulated data and the experimental measurements is excellent, at any value of water saturation. On the basis of these results, we can affirm that, while for porous media with a small surface conductivity (e.g., very low clay content) the approximation of two resistors in parallel is a reasonable assumption, in shaly sandstones this assumption may fail at some value of water saturation. By means of the above simulations, we also conclude that the contribution of surface conductivity is constant in the whole range of s_w investigated.

[49] We also modeled the effective real permittivity using the same code developed to compute electrical conductivity in the first approach. We calibrated a value of grain permittivity, which is in the ranges reported in literature for the solid matrix of natural porous media. Simulated and experimental measurements of the relationship between volumetric moisture content and effective permittivity show a very good match. This means that the effective permittivity depends on the property of the volume of the porous medium, and the effects of surface polarization can be considered negligible, while electrical conductivity strongly depends on the properties of the surface.

[50] The presented pore-scale models allowed us to investigate the electrical behavior of a porous medium at a local scale, comparing different mechanisms proposed in literature. This could be a powerful tool to investigate at a pore-scale the effects of several system parameters on electrical response of a porous medium, providing new constitutive relationships to be used in field applications.

[51] **Acknowledgments.** This work was supported by the Consorzio Interuniversitario CINECA (Bologna, Italy) and partly by the U.K. Natural Environment Research Council (NER/A/S/2001/00411). We thank Casey Miller (University of North Carolina, Chapel Hill, USA) and the University of North Carolina's pore-scale modeling group for providing us with the codes and for sharing their knowledge with us. We are very grateful to André Revil for helpful discussions and suggestions.

References

Archie, G. E. (1942), The electrical resistivity log as an aid in determining some reservoir characteristics, *Trans. Am. Inst. Min. Metall. Pet. Eng.*, *146*, 54–67.

Benson, A. K., K. L. Payne, and M. Stubben (1997), Mapping groundwater contamination using dc resistivity and vlf geophysical methods—A case study, *Geophysics*, *62*, 80–86.

Berg, C. R. (1995), A simple, effective-medium model for water saturation in porous rocks, *Geophysics*, *60*, 1070–1080.

Bernabé, Y., and A. Revil (1995), Pore scale heterogeneity, energy dissipation and the transport properties of rocks, *Geophys. Res. Lett.*, *22*(12), 1529–1532.

Binley, A., G. Cassiani, R. Middleton, and P. Winship (2002a), Vadose zone model parametrisation using cross-borehole radar and resistivity imaging, *J. Hydrol.*, *267*, 147–159.

Binley, A., P. Winship, J. West, M. Pokar, and R. Middleton (2002b), Seasonal variation of moisture content in unsaturated sandstone inferred from borehole radar and resistivity profiles, *J. Hydrol.*, *267*, 160–172.

Bussian, A. (1983), Electrical conductance in porous medium, *Geophysics*, *48*, 1258–1268.

Cassiani, G., C. Strobbia, and L. Gallotti (2004), Vertical radar profiles for the characterization of the deep vadose zone, *Vadose Zone J.*, *3*, 1093–1115.

Chan, C. Y., and R. J. Knight (1999), Determining water content from dielectric measurements in layered materials, *Water Resour. Res.*, *35*, 85–93.

Chelidze, T., and Y. Guéguen (1999), Electrical spectroscopy of porous rocks: A review—I. Theoretical models, *Geophys. J. Int.*, *137*, 1–15.

Chen, Y., L. Durlofsky, M. Gerritsen, and X. Wen (2003), A coupled local-global upscaling approach for simulating flow in highly heterogeneous formations, *Adv. Water Res.*, *26*, 1041–1060.

Chinh, P. D. (2000), Electrical properties of sedimentary rocks having interconnected water saturated pore space, *Geophysics*, *65*, 1093–1097.

Clavier, C., G. Coates, and J. Dumanoir (1985), The theoretical and experimental bases for the "dual water" model for the interpretation of shaly sands, *Soc. Pet. Eng. J.*, *24*, 153–169.

Daily, W., A. L. Ramirez, D. J. LaBrecque, and J. Nitao (1992), Electrical resistivity tomography of vadose water movement, *Water Resour. Res.*, *28*, 1429–1442.

Dalla, E., M. Hilpert, and C. Miller (2002), Computation of the interfacial area for two-fluid porous medium systems, *J. Contam. Hydrol.*, *56*, 25–48.

Dalla, E., G. Cassiani, A. Brovelli, and D. Pitea (2004), Electrical conductivity of unsaturated porous media: Pore-scale model and comparison with laboratory data, *Geophys. Res. Lett.*, *31*, L05609, doi:10.1029/2003GL019170.

De Lima, O., and M. Sharma (1990), A grain conductivity approach to shaly sandstones, *Geophysics*, *55*, 1347–1356.

Durlofsky, L., R. Jones, and W. Milliken (1997), A nonuniform coarsening approach for the scale-up of displacement processes in heterogeneous porous media, *Adv. Water Res.*, *20*, 335–347.

Endres, A. L., and R. Knight (1991), The effects of pore-scale fluid distribution on the physical properties of partially saturated tight sandstones, *J. Appl. Phys.*, *69*(2), 1091–1098.

Friedman, S. P. (1998), A saturation degree-dependent composite spheres model for describing the effective dielectric constant of unsaturated porous media, *Water Resour. Res.*, *34*(11), 2949–2961.

Glover, P., J. Malcom, and J. Pous (2000), A modified Archie's law for two conducting phases, *Earth Planet. Sci. Lett.*, *180*, 369–383.

Grant, I., and W. Phillips (1990), *Electromagnetism*, 2nd ed., John Wiley, Hoboken, N. J.

Guéguen, Y., and V. Palciauskas (1994), *Introduction to the Physics of Rocks*, Princeton Univ. Press.

Hilfer, H., J. Widjajakusuma, and B. Biswal (2000), Macroscopic dielectric constant for microstructures of sedimentary rocks, *Granular Matter*, *2*, 137–141.

Hilpert, M., and C. Miller (2001), Pore morphology based simulations of drainage in totally wetting porous media, *Adv. Water Resour.*, *24*, 243–255.

Johnson, D., J. Koplik, and L. M. Schwartz (1986), New pore-size parameter characterizing transport in porous media, *Phys. Rev. Lett.*, *57*, 2564–2567.

Jones, S. B., and S. P. Friedman (2000), Particle shape effects on the effective permittivity of anisotropic or isotropic media consisting of aligned or randomly oriented ellipsoidal particles, *Water Resour. Res.*, *36*(10), 2821–2833.

Kalinski, R., W. Kelly, I. Bogardi, and G. Pesti (1993), Electrical resisitivity measurements to estimate travel times through unsaturated ground water protective layers, *J. Appl. Geophys.*, *30*, 161–173.

Knight, R. (1991), Hysteresis in the electrical resistivity of partially saturated sandstones, *Geophysics*, *56*, 2139–2147.

Knight, R. J., and A. Nur (1987), The dielectric constant of sandstones, 60 khz to 4 Mhz, *Geophysics*, *52*, 644–657.

Korringa, J. (1984), The influence of pore geometry on the dielectric dispersion of clean sandstone, *Geophysics*, *49*, 1760–1762.

Kowalsky, M. B., S. Finsterle, and Y. Rubin (2004), Estimating flow parameter distributions using ground-penetrating radar and hydrological measurements during transient flow in the vadose zone, *Adv. Water Resour.*, *27*, 583–599.

Kuntz, M., J. C. Mareschal, and P. Lavallee (2000), Numerical estimation of electrical conductivity in saturated porous media with a 2-D lattice gas, *Geophysics*, *65*, 766–772.

Lorensen, W., and H. Cline (1987), Marching cubes: A high resolution 3D surface construction algorithm, *Comput. Graphics*, *21*(4), 163–169.

Man, H. N., and X. D. Jing (2001), Network modelling of strong and intermediate wettability on electrical resistivity and capillary pressure, *Adv. Water Res.*, *24*, 345–363.

Nettelblad, B., B. Ahlen, G. Niklasson, and R. Holt (1995), Approximate determination of surface conductivity in porous media, *J. Phys. D. Appl. Phys.*, *28*, 2037–2045.

O'Konski, C. (1960), Electric properties of macromolecules. v. Theory of ionic polarization in polyelectrolytes, *J. Phys. Chem.*, *64*, 605–619.

Revil, A., and P. Glover (1997), Theory of ionic-surface electrical conduction in porous media, *Phys. Rev. B*, *55*(3), 1757–1773.

Revil, A., L. Cathles, III, S. Losh, and J. Nunn (1998), Electrical conductivity in shaly sands with geophysical applications, *J. Geophys. Res.*, *103*(B10), 23,925–23,936.

Robinson, D., and S. P. Friedman (2003), A method for measuring the solid particle permittivity or electrical conductivity of rocks, sediments, and granular materials, *J. Geophys. Res.*, *108*(B2), 2076, doi:10.1029/2001JB000691.

Roth, K., R. Schulin, H. Fluhler, and W. Hattinger (1990), Calibration of time domain reflectometry for water content measurements using a composite dielectric approach, *Water Resour. Res.*, *26*(10), 2267–2273.

Sen, P., C. Scala, and M. Cohen (1981), A self-similar model for sedimentary rocks with application to the dielectric constant of fused glass beads, *Geophysics*, *46*, 781–795.

Suman, R. J., and R. J. Knight (1997), Effects of pore structure and wettability on electrical resistivity of partially saturated rocks—A network study, *Geophysics*, *62*, 1151–1162.

Taylor, S., and R. Barker (2002), Resistivity of partially saturated triassic sandstone, *Geophys. Prospect.*, *50*, 603–613.

Topp, G., J. Davis, and A. Annan (1980), Electromagnetic determination of soil water content: Measurement in coaxial transmission lines, *Water Resour. Res.*, *16*(3), 574–582.

Tsakiroglou, C. D., and M. Fleury (1999), Pore network analysis of resistivity index for water wet porous media, *Transp. Porous Media*, *35*, 89–128.

Waxman, M., and L. Smits (1968), Electrical conductivities in oil-bearing shaly sands, *Soc. Pet. Eng. J.*, *8*, 107–122.

West, L., K. Handley, Y. Huang, and M. Pokar (2003), Radar frequency dispersion in sandstone: Implication for the determination of the moisture and clay content, *Water Resour. Res.*, *39*(2), 1026, doi:10.1029/2001WR000923.

Wildenschild, D., J. Roberts, and E. Carlberg (2000), On the relationship between microstructure and electrical and hydraulic properties of sand-clay mixtures, *Geophys. Res. Lett.*, *27*(19), 3085–3088.

Yang, A., C. Miller, and L. Turcoliver (1996), Simulation of correlated and uncorrelated random size spheres, *Phys. Rev. E*, *53*, 1516–1524.

F. Bergamini, A. Brovelli, E. Dalla, and D. Pitea, Department of Environmental Science, University of Milano-Bicocca, Piazza della Scienza 1, 20126 Milano, Italy. (alessandro.brovelli@unimib.it)

A. M. Binley, Department of Environmental Science, Lancaster University, Lancaster LA1 4YQ, UK.

G. Cassiani, Department of Geology and Geosciences, University of Milano-Bicocca, Piazza della Scienza 4, 20126 Milano, Italy.